B19

A Monotone Non-linear Finite Volume Method for Advection-diffusion Equations and Multiphase Flows

K. Nikitin* (Institute of Numerical Mathematics RAS) & Y. Vassilevski (Institute of Numerical Mathematics RAS)

SUMMARY

We present a new nonlinear monotone finite volume method for diffusion and convection-diffusion equations and its application to two-phase black oil models. We consider full anisotropic discontinuous diffusion/permeability tensors and discontinuous velocity fields on conformal polyhedral meshes. The approximation of the diffusive flux uses the nonlinear two-point stencil which reduces to the conventional 7-point stencil for cubic meshes and diagonal tensors. The approximation of the advective flux is based on the second-order upwind method with the specially designed minimal nonlinear correction. We show that the quality of the discrete flux in a reservoir simulator has great effect on the front behavior and the water-breakthrough time. We compare the new nonlinear two-point flux discretization with the conventional linear two-point scheme. The new nonlinear scheme has a number of important advantages over the traditional linear discretization. First, it demonstrates low sensitivity to grid distortions. Second, it provides appropriate approximation in the case of full anisotropic permeability tensor. For non-orthogonal grids or full anisotropic permeability tensors the conventional linear scheme provides no approximation, while the nonlinear flux is still first-order accurate. The computational work for the new method is higher than the one for the conventional dicretization, yet it is rather competitive.

Introduction

Applications in reservoir simulation use different types of meshes such as tetrahedral, hexahedral, prismatic, octree, etc. All of them fall in the class of conformal meshes with polyhedral cells. The demand from the engineering community for a simple and accurate conservative method applicable to general conformal meshes and anisotropic tensor diffusion coefficients, is very distinct.

The conservative linear methods on unstructured meshes are well known: the multipoint flux approximation, MPFA (Aavatsmark et al. 2008), the mixed finite element, MFE (Brezzi and Fortin 1991) and the mimetic finite difference, MFD (Lipnikov and Gyrya 2008) methods. They are second-order accurate and are not monotone even when the diffusion coefficient is moderately (1:100) anisotropic. The cell-centered finite volume (FV) method with a linear two-point flux approximation is monotone but not even first-order accurate for anisotropic problems or unstructured meshes. Nevertheless, this method is conventional in modeling flows in porous media due to technological simplicity and monotonicity.

In this paper we present a new cell-centered finite volume method that preserves solution positivity and its application for multiphase flows. The method belongs to the class of methods with nonlinear flux discretizations (LePotier 2005; Kapyrin 2007; Lipnikov et al. 2007; Yuan and Sheng 2008; Vassilevski and Kapyrin 2008; Danilov and Vassilevski 2009; Lipnikov et al. 2009; Lipnikov et al. 2010; Nikitin and Vassilevski 2010). The method is applicable to the 3D conformal polyhedral meshes and diffusion equations with heterogeneous full diffusion tensor (Danilov and Vassilevski 2009). The method is applicable also to the convection-diffusion equations (Lipnikov et al. 2010; Nikitin and Vassilevski 2010). The approximation of advective fluxes is based on the upwinding approach along with a piecewise linear reconstruction of the FV solution and a slope limiting technique. In all cases of model equations, the method is exact for linear and piecewise linear solutions and thus has the second order truncation error. We note that the latest modification of the method (Lipnikov et al. 2012) provides the discrete maximum principle (DMP) and preserves the minimal compact stencil of the discretization.

The new nonlinear two-point flux discretization has a number of important advantages over conventional linear two-point flux discretization. First, it demonstrates very low sensitivity to grid distortions. Second, it provides appropriate approximations in the case of full anisotropic permeability (diffusion) tensor. Third, being combined with the cell-centered FV method, it preserves solution positivity and thus provides a monotone discretization.

The two-point support flux discretization methods are technologically appealing due to the compact stencil even on polygonal or polyhedral meshes. For cubic meshes and a diagonal diffusion tensor this stencil reduces to the conventional 7-point stencil. The major computational overhead in the nonlinear FV method is related to two nested iterations in the solution of a nonlinear algebraic problem. The outer iteration is the Picard method which guarantees solution positivity on each iteration. The inner iteration is the Krylov subspace method for solving linearized problems.

We consider applications of the new finite volume method to the solution of the black oil equations (Nikitin 2010). The two-phase black oil model concerns the secondary stage of oil recovery which is called water flooding. At this stage, water is injected into injection wells while oil is produced through production wells. We simulate the two-phase flow of immiscible fluids using the IMPES and fully implicit methods. The IMPES method presumes the discretization and solution of the diffusion equation for pressure. The implicit method presumes the straightforward discretization of the system of black oil equations. We show that the quality of the discrete flux in a reservoir simulator has a great effect on the front behavior and the water breakthrough time. We compare two methods of the discrete flux definition: the conventional linear two-point flux discretization and our nonlinear two-point flux discretization.

We emphasize that in special cases of orthogonal grid with isotropic or grid-aligned anisotropic permeability tensor the linear and nonlinear discretizations are identical. On the other hand, if the grid is not

orthogonal or the permeability tensor is anisotropic and rotated, the linear flux provides no approximation, while the nonlinear flux is still first-order accurate. The comparison study presented here shows several numerical experiments with two-phase black oil model that demonstrate significant loss of accuracy due to the conventional linear two-point flux discretization and justify the use of the nonlinear alternative.

The paper outline is as follows. In the first section we introduce the finite volumes method and different aproaches for the diffusive and advective flux discretizations. In the second section we remind the black oil model formulation and two time discretization schemes: IMPES and fully implicit method. In the third section we present the numerical results for the multiphase flows modeling using the conventional linear and new nonlinear flux discretization schemes.

Finite volumes method

First of all we remind the finite volumes method and introduce flux discretization schemes. Let Ω be a three-dimensional polyhedral domain with boundary consisting of two parts: $\Gamma = \Gamma_N \cup \Gamma_D$ and $\Gamma_D \cap \Gamma_N = \emptyset$.

We consider a model convection-diffusion problem for unknown concentration c:

$$\begin{aligned} \operatorname{div}(\mathbf{v}c - \mathbb{K}\nabla c) &= g && \text{in} && \Omega, \\ c &= g_D && \text{on} && \Gamma_D, \\ -(\mathbb{K}\nabla c)\cdot\mathbf{n} &= g_N && \text{on} && \Gamma_N, \end{aligned} \tag{1}$$

where $\mathbb{K}(\mathbf{x}) = \mathbb{K}^T(\mathbf{x}) > 0$ is a symmetric positive definite discontinuous (possibly anisotropic) full diffusion tensor, $\mathbf{v}(\mathbf{x})$ is a velocity field, div $\mathbf{v} \geq 0$, g is a source term, and $\mathbf{n}$ is the exterior normal vector.

Let $\mathscr{T}$ be a conformal polyhedral mesh composed of $N_{\mathscr{T}}$ shape-regular cells with planar faces and $N_{\mathscr{B}}$ boundary faces. We assume that each cell T is a star-shaped 3D domain with respect to its barycenter $\mathbf{x}_T$, and each face is a star-shaped 2D domain with respect to face's barycenter. We also assume that $\mathscr{T}$ is face-connected, i.e. it cannot be split into two meshes having no common faces.

Let $\mathbf{q}$ denote the total flux of a conservative unknown c which satisfies the mass balance equation for a source term g:

$$\operatorname{div}\mathbf{q} = g \quad \text{in} \quad \Omega. \tag{2}$$

We derive a FV scheme with a two-point flux approximation. Integrating equation (2) over a polyhedron T and using the Green's formula we get:

$$\int_{\partial T} \mathbf{q}\cdot\mathbf{n}_T \,\mathrm{d}s = \int_T g \,\mathrm{d}x, \tag{3}$$

where $\mathbf{n}_T$ denotes the outer unit normal to ∂T. Let f denote a face of cell T and $\mathbf{n}_f$ be the corresponding normal vector. For a single cell T, we always assume that $\mathbf{n}_f$ is the outward normal vector. In all other cases, we specify orientation of $\mathbf{n}_f$. It will be convenient to assume that $|\mathbf{n}_f| = |f|$ where $|f|$ denotes the area of face f. The equation (3) becomes

$$\sum_{f\in\partial T} \mathbf{q}_f\cdot\mathbf{n}_f = \int_T g \,\mathrm{d}x, \tag{4}$$

where $\mathbf{q}_f$ is the average flux density for face f.

For each cell T, we assign one degree of freedom, C_T, for the conservative unknown c. For simplicity, we shall refer to c as concentration. Let C be the vector of all discrete concentrations. If two cells T_+

and T_- have a common face f, our flux approximation with the two-point support, or the two-point flux approximation, is as follows:

$$\mathbf{q}_f^h \cdot \mathbf{n}_f = M_f^+ C_{T_+} - M_f^- C_{T_-}, \tag{5}$$

where M_f^+ and M_f^- are some coefficients. In a *linear* FV method, these coefficients are equal and fixed. In the *nonlinear* FV method, they may be different and depend on concentrations in surrounding cells. On face $f \in \Gamma_D$, the flux has a form similar to (5) with an explicit value for one of the concentrations. For the Dirichlet boundary value problem, $\Gamma_D = \partial\Omega$, substituting (5) into (4), we obtain a system of $N_{\mathscr{T}}$ equations with $N_{\mathscr{T}}$ unknowns C_T.

Therefore, the cornerstone of the cell-centered FV method is the definition of discrete flux (5). We combine the definition of the diffusive flux (Lipnikov et al. 2009; Danilov and Vassilevski 2009) and approximation of the advective flux based on the second-order upwind FV scheme (Lipnikov et al. 2010; Nikitin and Vassilevski 2010) and use them to construct an appropriate discretization for a black oil model.

Linear flux discretization

We consider non-orthogonal grid with anisotropic diffusion tensor: neither co-normal vectors $\mathbb{K}\mathbf{n}_f$, nor the vectors $\mathbf{t}_f$ connecting collocation points are orthogonal to faces (Fig. 1).

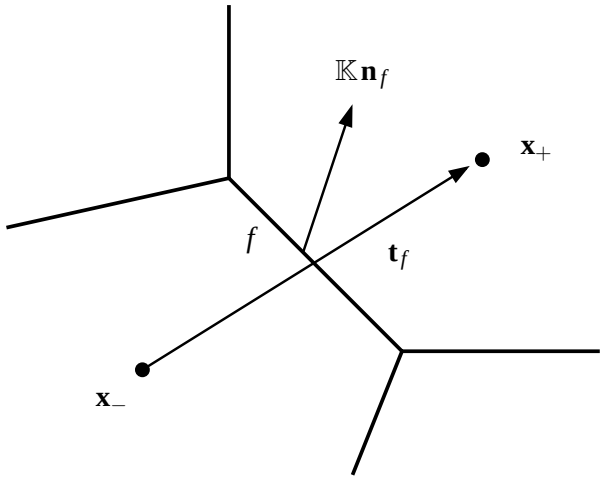

Figure 1 *Notations for the linear flux discretization.*

We assume that $|\mathbf{n}_f| = |f|$ and let $C_\pm = c(\mathbf{x}_\pm)$. For the flux through the interior face f we have:

$$\mathbb{K}\nabla c \cdot \mathbf{n}_f = \nabla c \cdot (\mathbb{K}\mathbf{n}_f). \tag{6}$$

The linear two-point discretization of the $\mathbf{t}_f$-component of the concentration gradient is:

$$(\nabla c)_{\mathbf{t}}^h = \frac{P_+ - P_-}{|\mathbf{t}_f|}. \tag{7}$$

Having $\nabla c \cdot (\mathbb{K}\mathbf{n}_f)$ as $(\nabla c)_{\mathbf{t}}^h \, (\mathbb{K}\mathbf{n}_f) \cdot \frac{\mathbf{t}_f}{|\mathbf{t}_f|}$ and substituting (7) into (6) we get

$$(\mathbb{K}\nabla c)_f^h \cdot \mathbf{n}_f = \frac{C_+ - C_-}{|\mathbf{t}_f|} \, \mathbb{K}\mathbf{n}_f \cdot \frac{\mathbf{t}_f}{|\mathbf{t}_f|} = \frac{\mathbb{K}\mathbf{n}_f \cdot \mathbf{t}_f}{|\mathbf{t}_f|^2} \, (C_+ - C_-) = \mathbb{T} \, (C_+ - C_-) \tag{8}$$

with the transmissibility $\mathbb{T} = \dfrac{\mathbb{K}\mathbf{n}_f \cdot \mathbf{t}_f}{|\mathbf{t}_f|^2}$.

The flux through the boundary edge is defined by the Dirichlet or Neumann data.

In the case of $\mathbb{K}$-orthogonal mesh, when $\mathbb{K}\mathbf{n}_f$ and $\mathbf{t}_f$ are collinear, the expression (8) takes the form of the central finite difference and approximates the flux with at least first order accuracy. But in general, the linear scheme may not provide approximation at all.

Nonlinear flux discretization

We consider the diffusive flux $\mathbf{q}_d = -\mathbb{K}\nabla c$.

Let $\mathscr{F}_I$, $\mathscr{F}_B$ be the disjoint sets of interior and boundary faces, respectively. The subset $\mathscr{F}_J$ of $\mathscr{F}_I$ collects faces with jumping diffusion tensor. The sets $\mathscr{F}_T$ and $\mathscr{E}_T$ denote the sets of faces and edges of polyhedron T, respectively. For every cell T in $\mathscr{T}$, we define the collocation point $\mathbf{x}_T$ at the barycenter of T. Finally, we denote by Σ_T the set of nearby collocation points of the cell T, and by $\Sigma_{f,T}$ the set of nearby collocation points of the face f belonging to the cell T.

We assume that for every cell-face pair $T \to f$, $T \in \mathscr{T}$, $f \in \mathscr{F}_T$, there exist three points $\mathbf{x}_{f,1}$, $\mathbf{x}_{f,2}$, and $\mathbf{x}_{f,3}$ in set Σ_T such that the following condition is held (see Fig. 2): The co-normal vector $\ell_f = \mathbb{K}(\mathbf{x}_f)\mathbf{n}_f$ started from $\mathbf{x}_T$ belongs to the trihedral corner formed by vectors

$$\mathbf{t}_{f,1} = \mathbf{x}_{f,1} - \mathbf{x}_T, \quad \mathbf{t}_{f,2} = \mathbf{x}_{f,2} - \mathbf{x}_T, \quad \mathbf{t}_{f,3} = \mathbf{x}_{f,3} - \mathbf{x}_T, \tag{9}$$

and

$$\frac{1}{|\ell_f|}\ell_f = \frac{\alpha_f}{|\mathbf{t}_{f,1}|}\mathbf{t}_{f,1} + \frac{\beta_f}{|\mathbf{t}_{f,2}|}\mathbf{t}_{f,2} + \frac{\gamma_f}{|\mathbf{t}_{f,3}|}\mathbf{t}_{f,3}, \tag{10}$$

where $\alpha_f \geq 0$, $\beta_f \geq 0$, $\gamma_f \geq 0$.

The coefficients α_f, β_f, γ_f are computed as follows:

$$\alpha_f = \frac{D_{f,1}}{D_f}, \qquad \beta_f = \frac{D_{f,2}}{D_f}, \qquad \gamma_f = \frac{D_{f,3}}{D_f}, \tag{11}$$

where

$$D_f = \frac{|\mathbf{t}_{f,1}\mathbf{t}_{f,2}\mathbf{t}_{f,3}|}{|\mathbf{t}_{f,1}||\mathbf{t}_{f,2}||\mathbf{t}_{f,3}|}, \quad D_{f,1} = \frac{|\ell_f\mathbf{t}_{f,2}\mathbf{t}_{f,3}|}{|\ell_f||\mathbf{t}_{f,2}||\mathbf{t}_{f,3}|}$$
$$D_{f,2} = \frac{|\mathbf{t}_{f,1}\ell_f\mathbf{t}_{f,3}|}{|\mathbf{t}_{f,1}||\ell_f||\mathbf{t}_{f,3}|}, \quad D_{f,3} = \frac{|\mathbf{t}_{f,1}\mathbf{t}_{f,2}\ell_f|}{|\mathbf{t}_{f,1}||\mathbf{t}_{f,2}||\ell_f|}$$

and $|\mathbf{a}\ \mathbf{b}\ \mathbf{c}| = |(\mathbf{a}\times\mathbf{b})\cdot\mathbf{c}|$.

Similarly, we assume that for every face-cell pair $f \to T$, $f \in \mathscr{F}_B \cup \mathscr{F}_J$, $T:\ f \in \mathscr{F}_T$ there exist three points $\mathbf{x}_{f,1}$, $\mathbf{x}_{f,2}$, and $\mathbf{x}_{f,3}$ in set $\Sigma_{f,T}$ such that the vector $\ell_{f,T} = -\mathbb{K}_T(\mathbf{x}_f)\mathbf{n}_f$ started from $\mathbf{x}_f$ belongs to the trihedral corner formed by vectors

$$\mathbf{t}_{f,1} = \mathbf{x}_{f,1} - \mathbf{x}_f, \quad \mathbf{t}_{f,2} = \mathbf{x}_{f,2} - \mathbf{x}_f, \quad \mathbf{t}_{f,3} = \mathbf{x}_{f,3} - \mathbf{x}_f, \tag{12}$$

and (10)-(11) hold true.

Let f be an interior face. We denote by T_+ and T_- the cells that share f and assume that $\mathbf{n}_f$ is outward for T_+. Let $\mathbf{x}_\pm$ (or $\mathbf{x}_{T_\pm}$) be the collocation points of $T_\pm$. Let $C_\pm$ (or $C_{T_\pm}$) be the discrete concentrations in $T_\pm$.

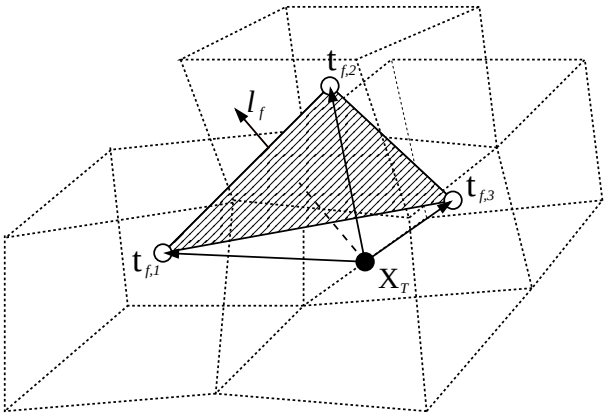

Figure 2 *Co-normal vector and vector triplet.*

We begin with the case $f \notin \mathscr{F}_J$ and introduce $\mathbb{K}_f = \mathbb{K}(\mathbf{x}_f)$. Let $T = T_+$. Using the above notations, definition of the directional derivative,

$$\frac{\partial c}{\partial \ell_f}|\ell_f| = \nabla c \cdot (\mathbb{K}_f \mathbf{n}_f),$$

and assumption (10), we write

$$\mathbf{q}_{f,d} \cdot \mathbf{n}_f \approx -\frac{|\ell_f|}{|f|}\int_f \frac{\partial c}{\partial \ell_f}\,\mathrm{d}s = -\frac{|\ell_f|}{|f|}\int_f \left(\alpha_f \frac{\partial c}{\partial \mathbf{t}_{f,1}} + \beta_f \frac{\partial c}{\partial \mathbf{t}_{f,2}} + \gamma_f \frac{\partial c}{\partial \mathbf{t}_{f,3}}\right)\mathrm{d}s. \tag{13}$$

Replacing directional derivatives by finite differences, we get

$$\int_f \frac{\partial c}{\partial \mathbf{t}_{f,i}}\,\mathrm{d}s = \frac{C_{f,i} - C_T}{|\mathbf{x}_{f,i} - \mathbf{x}_T|}\,|f| + O(h_T^3), \quad i = 1,2,3, \tag{14}$$

where h_T is the diameter of cell T. Using the finite difference approximations (14), we transform formula (13) to

$$\mathbf{q}^h_{f,d} \cdot \mathbf{n}_f = -|\ell_f|\left(\frac{\alpha_f}{|\mathbf{t}_{f,1}|}(C_{f,1} - C_T) + \frac{\beta_f}{|\mathbf{t}_{f,2}|}(C_{f,2} - C_T) + \frac{\gamma_f}{|\mathbf{t}_{f,3}|}(C_{f,3} - C_T)\right). \tag{15}$$

At the moment, this flux involves four rather than two concentrations. To derive a two-point flux approximation, we consider the cell T_- and derive another approximation of flux through face f. To distinguish between T_+ and T_-, we add subscripts $\pm$ and omit subscript f. Since $\mathbf{n}_f$ is the internal normal vector for T_-, we have to change sign of the right-hand side:

$$\mathbf{q}^h_{\pm,d} \cdot \mathbf{n}_f = \mp|\ell_f|\left(\frac{\alpha_\pm}{|\mathbf{t}_{\pm,1}|}(C_{\pm,1} - C_\pm) + \frac{\beta_\pm}{|\mathbf{t}_{\pm,2}|}(C_{\pm,2} - C_\pm) + \frac{\gamma_\pm}{|\mathbf{t}_{\pm,3}|}(C_{\pm,3} - C_\pm)\right), \tag{16}$$

where $\alpha_\pm$, $\beta_\pm$ and $\gamma_\pm$ are given by (11) and $C_{\pm,i}$ denote concentrations at points $\mathbf{x}_{\pm,i}$ from $\Sigma_{T_\pm}$.

We define a new discrete diffusive flux as a linear combination of $\mathbf{q}^h_{\pm,d} \cdot \mathbf{n}_f$ with non-negative weights $\mu_\pm$:

$$\begin{aligned}
\mathbf{q}^h_{f,d} \cdot \mathbf{n}_f &= \mu_+ \mathbf{q}^h_+ \cdot \mathbf{n}_f + \mu_- \mathbf{q}^h_- \cdot \mathbf{n}_f \\
&= \mu_+|\ell_f|\left(\frac{\alpha_+}{|\mathbf{t}_{+,1}|} + \frac{\beta_+}{|\mathbf{t}_{+,2}|} + \frac{\gamma_+}{|\mathbf{t}_{+,3}|}\right)C_+ - \mu_-|\ell_f|\left(\frac{\alpha_-}{|\mathbf{t}_{-,1}|} + \frac{\beta_-}{|\mathbf{t}_{-,2}|} + \frac{\gamma_-}{|\mathbf{t}_{-,3}|}\right)C_- \\
&- \mu_+|\ell_f|\left(\frac{\alpha_+}{|\mathbf{t}_{+,1}|}C_{+,1} + \frac{\beta_+}{|\mathbf{t}_{+,2}|}C_{+,2} + \frac{\gamma_+}{|\mathbf{t}_{+,3}|}C_{+,3}\right) \\
&+ \mu_-|\ell_f|\left(\frac{\alpha_-}{|\mathbf{t}_{-,1}|}C_{-,1} + \frac{\beta_-}{|\mathbf{t}_{-,2}|}C_{-,2} + \frac{\gamma_-}{|\mathbf{t}_{-,3}|}C_{-,3}\right).
\end{aligned} \tag{17}$$

The obvious requirement for the weights is to cancel the terms in the last two rows of (17) which results in a two-point flux formula. The second requirement is to approximate the true flux. These requirements lead us to the following system

$$\begin{cases} -\mu_+ d_+ + \mu_- d_- &= 0, \\ \mu_+ + \mu_- &= 1, \end{cases} \tag{18}$$

where

$$d_\pm = |\ell_f| \left(\frac{\alpha_\pm}{|\mathbf{t}_{\pm,1}|} C_{\pm,1} + \frac{\beta_\pm}{|\mathbf{t}_{\pm,2}|} C_{\pm,2} + \frac{\gamma_\pm}{|\mathbf{t}_{\pm,3}|} C_{\pm,3} \right).$$

Since coefficients $d_\pm$ depend on both geometry and concentration, the weights $\mu_\pm$ do as well. Thus, the resulting two-point flux approximation is *nonlinear*.

Remark 1. *It may happen that concentration $C_{+,i}$, ($C_{-,i}$) $i = 1,2,3$, is defined at the same collocation point as C_- (C_+). In this case the terms to be cancelled are changed so that they do not incorporate $C_\pm$. By doing so, for the Laplace operator we recover the classical linear scheme with the 6-1-1-1-1-1-1 stencil on uniform cubic meshes.*

The solution of (18) can be written explicitly. In all cases $d_\pm \geq 0$ if $C \geq 0$. If $d_\pm = 0$, we set $\mu_+ = \mu_- = \frac{1}{2}$. Otherwise,

$$\mu_+ = \frac{d_-}{d_- + d_+} \qquad \text{and} \qquad \mu_- = \frac{d_+}{d_- + d_+}.$$

This implies that the weights $\mu_\pm$ are non-negative. Substituting this into (17), we get the two-point flux formula (5) with non-negative coefficients

$$\mathbf{q}^h_{f,d} \cdot \mathbf{n}_f = D^+_f C_{T_+} - D^-_f C_{T_-}, \tag{19}$$

$$D^\pm_f = \mu_\pm |\ell_f| (\alpha_\pm / |\mathbf{t}_{\pm,1}| + \beta_\pm / |\mathbf{t}_{\pm,2}| + \gamma_\pm / |\mathbf{t}_{\pm,3}|). \tag{20}$$

Now we consider the case $f \in \mathscr{F}_J$ when $\mathbb{K}_+(\mathbf{x}_f)$ and $\mathbb{K}_-(\mathbf{x}_f)$ differ, where

$$\mathbb{K}_\pm(\mathbf{x}_f) = \lim_{\mathbf{x} \in \mathscr{T}_\pm,\ \mathbf{x} \to \mathbf{x}_f} \mathbb{K}(\mathbf{x}).$$

We derive two-point flux approximations in cells T_+ and T_- independently:

$$(\mathbf{q}^h_{f,d} \cdot \mathbf{n}_f)_+ = N^+ C_+ - N^+_f C_f, \tag{21}$$

$$-(\mathbf{q}^h_{f,d} \cdot \mathbf{n}_f)_- = N^- C_- - N^-_f C_f. \tag{22}$$

Non-negative coefficients N^+, N^+_f, N^-, N^-_f are derived similarly to coefficients (20) on the basis of discrete concentrations at collocation points from $\Sigma_{T_\pm}$, $\Sigma_{f,T_\pm}$ and $\ell_\pm = \mp \mathbb{K}_\pm(\mathbf{x}_f)\,\mathbf{n}_f$, the co-normal vectors to face f outward with respect to $T_\pm$. Continuity of the normal component of the total flux and the advection field implies continuity of the normal component of the diffusive flux. This assertion allows us to eliminate C_f from (21)-(22)

$$C_f = (N^+ C_+ + N^- C_-)/(N^+_f + N^-_f) \tag{23}$$

and derive the two-point flux approximation (19) with coefficients

$$D^\pm_f = N^\pm N^\mp_f / (N^+_f + N^-_f). \tag{24}$$

If both $N^\pm_f = 0$, we set $M^\pm_f = N^\pm/2$ and $C_f = (C_+ + C_-)/2$.

Nonlinear second-order upwind stabilization

We consider the nonlinear upwind approximation for the conservative unknown c by the flux $\mathbf{v}$:

$$C_f = \begin{cases} \mathscr{R}_{T^+}(\mathbf{x}_f), & v_f > 0, \\ \mathscr{R}_{T^-}(\mathbf{x}_f), & else, \end{cases} \tag{25}$$

where

$$v_f = \frac{1}{|f|}\int_f \mathbf{v}\cdot\mathbf{n}_f \, ds,$$

$\mathscr{R}_T$ is a linear reconstruction of the concentration over cell T which depends on the concentration values from neighboring cells.

On each cell T we define the linear reconstruction

$$\mathscr{R}_T(\mathbf{x}) = \begin{cases} C_T + \mathscr{L}_T \mathbf{g}_T \cdot (\mathbf{x}-\mathbf{x}_T), & \mathbf{x}\in T, \\ 0, & \mathbf{x}\notin T, \end{cases} \tag{26}$$

with a gradient vector $\mathbf{g}_T$. Since C_T is collocated at the barycenter of T, this reconstruction preserves the mean value of the concentration for any choice of $\mathbf{g}_T$.

Conventional reconstructions of the gradient target stable approximations of the second order. Let $\mathscr{G}_T$ be the set of admissible gradients $\tilde{\mathbf{g}}_T$ which will be defined below. The gradient vector $\mathbf{g}_T$ is the solution to the following constrained minimization problem:

$$\mathbf{g}_T = \arg\min_{\tilde{\mathbf{g}}_T\in\mathscr{G}_T} \mathscr{J}_T(\tilde{\mathbf{g}}_T), \tag{27}$$

where the functional

$$\mathscr{J}_T(\tilde{\mathbf{g}}_T) = \frac{1}{2}\sum_{\mathbf{x}_k\in\tilde{\Sigma}_T} [C_T + \tilde{\mathbf{g}}_T\cdot(\mathbf{x}_k-\mathbf{x}_T) - C_k]^2$$

measures deviation of the reconstructed function from the targeted values C_k collocated at points $\mathbf{x}_k$ from a set $\tilde{\Sigma}_T$. The set $\tilde{\Sigma}_T$ is built as follows. First, the set $\hat{\Sigma}_T$ is defined by eliminating the secondary collocation points $\mathbf{x}_f$, $f\in\mathscr{F}_B^{out}$, from Σ_T. Second, we set $\tilde{\Sigma}_T = \hat{\Sigma}_T$ and extend it by elements from $\tilde{\Sigma}_{T'}$, for all $T'\neq T$ s.t. $\mathbf{x}_{T'}\in\tilde{\Sigma}_T$, if the least-square system is degenerate or ill-conditioned.

The set of admissible gradients $\mathscr{G}_T$ is defined via three constraints suppressing non-physical oscillations. These constraints (as well as the set $\tilde{\Sigma}_T$) were designed to be practical and at the same time as weak as possible. First, a linear reconstruction defined by the admissible gradient $\tilde{\mathbf{g}}_T$ must be bounded at the collocation points $\mathbf{x}_k\in\hat{\Sigma}_T$:

$$\min\left\{C_1, C_2, \ldots, C_{N(\hat{\Sigma}_T)}\right\} \le C_T + \tilde{\mathbf{g}}_T\cdot(\mathbf{x}_k-\mathbf{x}_T) \le \max\left\{C_1, C_2, \ldots, C_{N(\hat{\Sigma}_T)}\right\}. \tag{28}$$

Due to (28), we get that $\tilde{\mathbf{g}}_T\equiv 0$ in local minima and maxima.

Second, for the sake of the correct sign of the advective flux, we require that the reconstructed function must be non-negative at points $\mathbf{x}_f$ on faces $f\in\mathscr{F}_T$ where $v_f>0$:

$$C_T + \tilde{\mathbf{g}}_T\cdot(\mathbf{x}_f-\mathbf{x}_T) \ge 0. \tag{29}$$

We note that when the face center $\mathbf{x}_f$ lies outside the convex hull of points $\mathbf{x}_k\in\hat{\Sigma}_T$, the reconstructed function may be negative at $\mathbf{x}_f$ even if (28) is satisfied.

Third, the reconstructed function must be bounded from below at the secondary collocation points on Γ_{out} (they do not belong to $\hat{\Sigma}_T$):

$$\min\left\{C_1, C_2, \ldots, C_{N(\hat{\Sigma}_T)}\right\} \le C_T + \tilde{\mathbf{g}}_T\cdot(\mathbf{x}_f-\mathbf{x}_T), \qquad f\in\mathscr{F}_T\cap\mathscr{F}_B^{out}. \tag{30}$$

Ignoring constraint (30) can involve difficulties in the solution of resulting nonlinear algebraic system.

It can be proved (Nikitin and Vassilevski 2010; Lipnikov et al. 2010) that minimization problem (27) with constraints (28), (29), (30) has a unique solution.

The resulting reconstruction (26) can be used for the advective flux discretization as well as for the second order nonlinear upwind approximation of the conservative unknown c.

Nonlinear discrete system and its solution

For every T in $\mathscr{T}$, the cell equation (4) is

$$\sum_{f\in\mathscr{F}_T} \chi(T,f)\,\mathbf{q}_f^h\cdot\mathbf{n}_f = \int_T f\,\mathrm{d}x, \tag{31}$$

where $\chi(T,f) = sign(\mathbf{n}_f\cdot\mathbf{n}_T(\mathbf{x}_f))$. Substituting two-point flux formula (5) with non-negative coefficients given by (20) and (24) into (31), we get a nonlinear system of $N_{\mathscr{T}}$ equations

$$\mathbf{M}(C)C = G(C). \tag{32}$$

The matrix $\mathbf{M}(C)$ may be represented by assembling of 2×2 matrices

$$\mathbf{M}_f(C) = \begin{pmatrix} M_f^+(C) & -M_f^-(C) \\ -M_f^+(C) & M_f^-(C) \end{pmatrix} \tag{33}$$

for the interior faces and 1×1 matrices $\mathbf{M}_f(C) = M_f^+(C)$ for Dirichlet faces. The right-hand side vector $G(C)$ is generated by the source and the boundary data.

We use the Picard iterations to solve the nonlinear system (32). Each Picard iteration produce the linear system with the non-symmetric matrix $\mathbf{M}(\mathbf{C}^k)$ can be solved by, for example, the preconditioned Bi-Conjugate Gradient Stabilized (BiCGStab) method. The BiCGStab iterations are terminated when the relative norm of the residual becomes smaller than ε_{lin}.

The next two theorems (Lipnikov et al. 2010) show that the solution to (32) is non-negative provided that it exists and that the solution C^k for each k^{th} Picard iteration is a non-negative vector provided that $\varepsilon_{lin} = 0$.

Theorem 1. *Let $\Gamma_N = \emptyset$, $g \geq 0$ in Ω, $g_D \geq 0$ on $\Gamma_D \equiv \partial\Omega$ and the solution C to* (32) *exist. Then $C \geq 0$.*

Theorem 2. *Let $g \geq 0$, $g_D \geq 0$, $g_N \leq 0$ and $\Gamma_D \neq \emptyset$. If $\mathbf{C}^0 \geq 0$ and linear systems in the Picard method are solved exactly, then $\mathbf{C}^k \geq 0$ for $k \geq 1$.*

Remark 2. *The presented FV method is exact for piecewise linear concentrations and has the second order truncation error. Therefore, we may expect the second order of convergence for the scalar variable C and at least the first order of convergence for the flux degrees of freedom.*

Two-phase black oil model

For the sake of simplicity we consider a two-phase flow in a porous medium (Aziz and Settari 1979; Chen et al. 2006), as for the three-phase flow the effect of using linear or nonlinear discretization scheme is the same. The phase, that wets the medium more than the other, is called wetting phase and is indicated by subscript w. The other phase is the nonwetting phase and indicated by o.

The basic equations for the two-phase flow are the following:

- Mass conservation for each phase:

$$\frac{\partial}{\partial t}(\phi\rho_\alpha S_\alpha) = -\mathrm{div}(\rho_\alpha\mathbf{u}_\alpha) + q_\alpha, \quad \alpha = w,o \tag{34}$$

- Darcy's law:

$$\mathbf{u}_\alpha = -\frac{k_{r\alpha}}{\mu_\alpha}\mathbb{K}(\nabla p_\alpha - \rho_\alpha g \nabla z), \quad \alpha = w, o \tag{35}$$

- Two fluids fill the voids:

$$S_w + S_o = 1 \tag{36}$$

- Pressure difference between phases is given by capillary pressure:

$$p_o - p_w = p_c(S_w) \tag{37}$$

where p_α is unknown phase pressure α, S_α is unknown saturation, $\mathbf{u}_\alpha$ is unknown Darcy's velocity, $\mathbb{K}$ is an absolute permeability tensor, $\rho_\alpha = \rho_{\alpha,0}/B_\alpha$ is a phase density, with $\rho_{\alpha,0}$ being a density under standard conditions, $B_\alpha = B_\alpha(p)$ is a formation volume factor, $\mu_\alpha = \mu_\alpha(p)$ is a viscosity, $k_{r\alpha} = k_{r\alpha}(S)$ is a relative phase permeability, $\phi = \phi(p)$ is a porosity, g is a gravity term, z is a depth and q_α is a source/sink well term.

Boundary conditions consist of two parts:

1. No-flow (homogeneous Neumann) condition on the reservoir boundary;
2. Wells with a given bottom pressure p_{bh}.

Each well is assumed to be vertical and connected to the center of a cell. The formula for the well term was suggested by Peaceman (Peaceman 1978):

$$q_\alpha = \frac{\rho_\alpha k_{r\alpha}}{\mu_\alpha} WI(p_{\text{bh}} - p - \rho_\alpha(z_{\text{bh}} - z)), \tag{38}$$

where WI is a well index, which doesn't depend on the properties of fluids, but depends on properties of the media.

In the discrete counterpart of (43), (44), (45) the mobility $\lambda_\alpha = \frac{k_{r\alpha}(S_w)}{\mu_\alpha(p_o)}$ on face f_{ij} is taken upwinded:

$$\lambda_\alpha(S) = \begin{cases} \lambda_\alpha(S_i) & \text{if flow is directed from cell } i \text{ to cell } j, \\ \lambda_\alpha(S_j) & \text{if flow is directed from cell } j \text{ to cell } i. \end{cases}$$

The phase mobilities for well-producer are taken upwinded from the cell. For well-injector we have only water injected and thus take the downstream mobility from the cell with the well:

$$\lambda_{\text{injector}} = \left(\frac{k_{rw}}{\mu_w} + \frac{k_{ro}}{\mu_o}\right)_{\text{cell}}.$$

It is assumed that there is no capillary pressure in wells, so both water and oil fluxes depend on the same (oil) pressure.

IMPES time stepping

In this section we derive the IMPES (Implicit Pressure – Explicit Saturation) time stepping for two-phase black oil model. The oil pressure and water saturation are chosen as independent variables:

$$p = p_o, \quad S = S_w.$$

The total velocity is $\mathbf{u} = \mathbf{u}_o + \mathbf{u}_w$.

If the rock porosity and liquid densities are fixed during the time step, we have

$$\frac{\partial(\phi S_o)}{\partial t} + \frac{\partial(\phi S_w)}{\partial t} = 0$$

and then

$$\nabla \cdot \mathbf{u} = \frac{q_w}{\rho_w} + \frac{q_o}{\rho_o} \tag{39}$$

Applying (37) to (35) gives

$$\mathbf{u} = -\mathbb{K}\big(\lambda(S)\nabla p - \lambda_w(S)\nabla p_c - (\lambda_w\rho_w + \lambda_o\rho_o)g\nabla z\big), \tag{40}$$

where $\lambda = \lambda_w + \lambda_o$ is the total mobility.

Substituting (40) into (39) gives the pressure equation

$$-\nabla\cdot(\mathbb{K}\lambda\nabla p) = \frac{q_w}{\rho_w} + \frac{q_o}{\rho_o} - \nabla\cdot\big[\mathbb{K}\big(\lambda_w\nabla p_c + (\lambda_w\rho_w + \lambda_o\rho_o)g\nabla z\big)\big]. \tag{41}$$

The phase velocities $\mathbf{u}_w$ and $\mathbf{u}_o$ can be expressed through the total velocity $\mathbf{u}$ by

$$\mathbf{u}_w = \frac{\lambda_w}{\lambda}\big(\mathbf{u} + \mathbb{K}\lambda_o\nabla p_c + \mathbb{K}\lambda_o(\rho_w - \rho_o)g\nabla z\big),$$

$$\mathbf{u}_o = \frac{\lambda_o}{\lambda}\big(\mathbf{u} - \mathbb{K}\lambda_w\nabla p_c + \mathbb{K}\lambda_w(\rho_o - \rho_w)g\nabla z\big).$$

Similarly, (37) and (40) applied to (34) and (35) (for $\alpha = w$) yield the saturation equation

$$\phi\frac{\partial S}{\partial t} + \nabla\cdot\frac{\lambda_w}{\lambda}(S)\left[\mathbb{K}\lambda_o(S)\left(\frac{dp_c}{dS}\nabla S + (\rho_o - \rho_w)g\nabla z\right) + \mathbf{u}\right] = \frac{q_w}{\rho_w} \tag{42}$$

Finally, the IMPES method can be formalized:

1. Solve **implicitly** (41) to obtain current pressure p^n from current saturation S^n:

$$-\nabla\cdot(\mathbb{K}\lambda^n\nabla p^n) = \frac{q_w}{\rho_w^n} + \frac{q_o}{\rho_o^n} - \nabla\cdot\big[\mathbb{K}\big(\lambda_w^n\nabla p_c + (\lambda_w^n\rho_w^n + \lambda_o^n\rho_o^n)g\nabla z\big)\big], \tag{43}$$

   where $\lambda_\alpha^n = \lambda_\alpha(S^n, p^n)$ and $\rho_\alpha^n = \rho_\alpha(p^n)$.

2. Use (40) to find current Darcy's velocity $\mathbf{u}^n$ using current S^n and p^n:

$$\mathbf{u}^n = -\mathbb{K}\big(\lambda^n\nabla p^n - \lambda_w^n\nabla p_c - (\lambda_w^n\rho_w^n + \lambda_o^n\rho_o^n)g\nabla z\big). \tag{44}$$

3. Solve **explicitly** (42) to get next time step saturation S^{n+1} using current S^n, p^n and u^n:

$$\frac{1}{\Delta t^{n+1}}\left[\left(\frac{\phi S}{B_w}\right)^{n+1} - \left(\frac{\phi S}{B_w}\right)^n\right] = \frac{q_w}{\rho_w^n} - \nabla\cdot\frac{\lambda_w^n}{\lambda^n}\left[\mathbb{K}\lambda_o^n\left(\frac{dp_c}{dS}\nabla S + (\rho_o^n - \rho_w^n)g\nabla z\right) + \mathbf{u}^n\right]. \tag{45}$$

Note that the equation (43) is a stationary diffusion equation with diffusion tensor $\mathbb{K}\lambda^n$ and the nonlinear right-hand side. While forming diffusion fluxes on the left and right sides of the equation (43), as well as the right-hand sides of (44) and (45) we use a linear or nonlinear discretization scheme, which were introduced in the first section, substituting pressure instead of concentration.

Fully implicit scheme

Another time discretization technique widely used in reservoir simulation is the fully implicit scheme. First we apply the implicit scheme to the mass conservation equations (34):

$$\frac{\left(\frac{\phi S_\alpha}{B_\alpha}\right)^{n+1} - \left(\frac{\phi S_\alpha}{B_\alpha}\right)^{n}}{\Delta t^{n+1}} = -\mathrm{div}\left(\frac{\mathbf{u}_\alpha}{B_\alpha}\right)^{n+1} + \left(\frac{q_\alpha}{\rho_{\alpha,0}}\right)^{n+1}, \quad \alpha = w, o. \tag{46}$$

Now we can write down the nonlinear residual equations for the l^{th} approximation to a quantity evaluated at time step $n+1$ inside grid cell T_i:

$$R^l_{\alpha,i} = \int_{T_i} \left[\left(\frac{\phi S_\alpha}{B_\alpha}\right)^{l}_i - \left(\frac{\phi S_\alpha}{B_\alpha}\right)^{n}_i + \Delta t^{n+1} \left(\mathrm{div}\frac{\mathbf{u}_\alpha}{B_\alpha} - \frac{q_\alpha}{\rho_{\alpha,0}} \right)^{l}_i \right] \mathrm{d}x, \quad \alpha = w, o. \tag{47}$$

The discrete counterpart of (46) can be written as:

$$R_{\alpha,i} = 0, \quad \alpha = w, o \tag{48}$$

for all grid cells at every time step.

We suggest to use Newton's method to solve nonlinear system (48) with Darcy velocities (35):

$$J(x^l)\delta x^l = -R(x^l), \tag{49}$$

$$x^{l+1} = x^l + \delta x^l, \tag{50}$$

where l is the l^{th} Newton step, x is a vector of primary unknowns in all grid cells,

$$x = \begin{pmatrix} p_o \\ S_w \end{pmatrix},$$

R is the vector of nonlinear residuals in all grid cells,

$$R(x) = \begin{pmatrix} R_w(x) \\ R_o(x) \end{pmatrix},$$

and J is the Jacobian matrix:

$$J(x) = \begin{pmatrix} \frac{\partial R_w}{\partial p_o}(x) & \frac{\partial R_w}{\partial S_w}(x) \\ \frac{\partial R_o}{\partial p_o}(x) & \frac{\partial R_o}{\partial S_w}(x) \end{pmatrix}.$$

We terminate Newton's method when the norm of the residual vector drops below $\varepsilon_{\mathrm{nwt}}$.

Below we consider the construction of Jacobian matrix. We divide the residuals into two parts: accumulation (including well terms) and transport, $R_{\alpha,i} = R^{acc}_{\alpha,i} + R^{trans}_{\alpha,i}$, where:

$$R^{acc}_{\alpha,i} = V_i \left[\left(\frac{\phi S_\alpha}{B_\alpha}\right)^{l}_i - \left(\frac{\phi S_\alpha}{B_\alpha}\right)^{n}_i - \Delta t^{n+1} \left(\frac{q_\alpha}{\rho_{\alpha,0}}\right)^{l}_i \right], \quad \alpha = w, o,$$

$$R^{trans}_{\alpha,i} = \Delta t^{n+1} \int_{T_i} \left(\mathrm{div}\frac{\mathbf{u}_\alpha}{B_\alpha} \right) \mathrm{d}x, \quad \alpha = w, o.$$

We take advantage of the following dependencies:

- $S_o = 1 - S_w$, (rf. (36)),
- $p_w = p_o - p_c(S_w)$,
- $k_{r\alpha} = k_{r\alpha}(S_w)$,
- $\mu_\alpha = \mu_\alpha(p_o)$,
- $B_\alpha = B_\alpha(p_o)$,
- $\phi = \phi_0(1 + c_R(p_o - p_o^0))$.

Accumulation term.

First we consider the variation of the accumulation term:

$$\Delta R_{w,i}^{acc} = V_i \left[\Delta \left(\frac{\phi S_w}{B_w} \right) - \Delta t^{n+1} \Delta \left(\frac{q_w}{\rho_{w,0}} \right) \right],$$

$$\Delta R_{o,i}^{acc} = V_i \left[\Delta \left(\frac{\phi S_o}{B_o} \right) - \Delta t^{n+1} \Delta \left(\frac{q_o}{\rho_{o,0}} \right) \right],$$

where

$$\Delta \left(\frac{\phi S_w}{B_w} \right) = \frac{\phi}{B_w} \Delta S_w + S_w \left(\frac{\phi_0 c_R}{B_w} - \frac{\phi}{B_w^2} \frac{dB_w}{dp_o} \right) \Delta p_o,$$

$$\Delta \left(\frac{\phi S_o}{B_o} \right) = -\frac{\phi}{B_o} \Delta S_w + (1 - S_w) \left(\frac{\phi_0 c_R}{B_o} - \frac{\phi}{B_o^2} \frac{dB_o}{dp_o} \right) \Delta p_o.$$

For the production well we have:

$$\Delta \left(\frac{q_\alpha}{\rho_{\alpha,0}} \right) = \left(\frac{WI\, \mathscr{D}_\alpha}{\mu_\alpha B_\alpha} \right) \frac{dk_{r\alpha}}{dS_w} \Delta S_w - \frac{k_{r\alpha} WI}{\mu_\alpha B_\alpha} \left(1 + \mathscr{D}_\alpha \left(\frac{1}{\mu_\alpha} \frac{d\mu_\alpha}{dp_o} + \frac{1}{B_\alpha} \frac{dB_\alpha}{dp_o} \right) \right) \Delta p_o,$$

and for the injection well:

$$\begin{aligned} \Delta \left(\frac{q_w}{\rho_{w,0}} \right) = WI\, \mathscr{D}_w \left(\frac{1}{\mu_w B_w} \frac{dk_{rw}}{dS_w} + \frac{1}{\mu_o B_o} \frac{dk_{ro}}{dS_w} \right) \Delta S_w - WI \left[\frac{k_{rw}}{\mu_w B_w} + \frac{k_{ro}}{\mu_o B_o} + \right. \\ \left. + \mathscr{D}_w \left(\frac{k_{rw}}{\mu_w^2 B_w} \frac{d\mu_w}{dp_o} + \frac{k_{rw}}{\mu_w B_w^2} \frac{dB_w}{dp_o} + \frac{k_{ro}}{\mu_o^2 B_o} \frac{d\mu_o}{dp_o} + \frac{k_{ro}}{\mu_o B_o^2} \frac{dB_o}{dp_o} \right) \right] \Delta p_o, \end{aligned} \tag{51}$$

$$\Delta \left(\frac{q_o}{\rho_{o,0}} \right) = 0,$$

where $\mathscr{D}_\alpha = p_{\text{bh}} - p_o - \rho_\alpha (z_{\text{bh}} - z)$.

Transport term.

Now we consider the transport term composed of Darcy fluxes

$$R_{\alpha,i}^{trans} = \Delta t^{n+1} \int_{\partial T_i} \left(\frac{\mathbf{u}_\alpha}{B_\alpha} \cdot \mathbf{n} \right) \mathrm{d}s \approx \Delta t^{n+1} \sum_{f \in \partial T_i} \frac{\mathbf{u}_{\alpha,f}}{B_\alpha} \cdot \mathbf{n}_f. \tag{52}$$

Consider we have a two-point discretization for a flux. In this case

$$\begin{aligned} \frac{\mathbf{u}_{w,f}^h}{B_w} \cdot \mathbf{n}_f &= -\left(\frac{k_{rw}}{\mu_w B_w} \right)_f \left[D_f^+ \left(p_w - \rho_w g z \right)_{T_+} - D_f^- \left(p_w - \rho_w g z \right)_{T_-} \right] = \\ &= -\left(\frac{k_{rw}}{\mu_w B_w} \right)_f \left[D_f^+ \left(p_o - p_c(S_w) - \rho_w g z \right)_{T_+} - D_f^- \left(p_o - p_c(S_w) - \rho_w g z \right)_{T_-} \right], \end{aligned} \tag{53}$$

$$\frac{\mathbf{u}^h_{o,f}}{B_o}\cdot\mathbf{n}_f = -\left(\frac{k_{ro}}{\mu_o B_o}\right)_f \left[D_f^+\left(p_o-\rho_o g z\right)_{T_+} - D_f^-\left(p_o-\rho_o g z\right)_{T_-}\right]. \tag{54}$$

Here $k_{r\alpha} = k_{r\alpha}(\widetilde{S})$, $\widetilde{S}$ is the upwinded value of saturation on face f. On the other hand, $\mu_\alpha = \mu_\alpha(\bar{p})$ and $B_\alpha = B_\alpha(\bar{p})$, where $\bar{p} = \frac{p_- + p_+}{2}$ is the average pressure on the face.

Using (53) and (54) we get the following representation for the flux variation for each of two phases:

$$\begin{aligned}\Delta\left(\frac{\mathbf{u}^h_{w,f}}{B_w}\cdot\mathbf{n}_f\right) = {} & \frac{-\mathscr{D}_{w,f}}{\mu_w B_w}\frac{dk_{rw}}{S_w}\Delta\widetilde{S}_w - \\ & -\frac{k_{rw}}{\mu_w B_w}\left[-D_f^+\left(\frac{dp_c}{dS_w}\Delta S_w\right)_{T_+} + D_f^-\left(\frac{dp_c}{dS_w}\Delta S_w\right)_{T_-}\right] + \\ & +\frac{k_{rw}}{\mu_w B_w}\left[\left(\frac{\mathscr{D}_{w,f}}{\mu_w}\frac{d\mu_w}{dp_o} + \frac{\mathscr{D}_{w,f}}{B_w}\frac{dB_w}{dp_o}\right)\Delta\bar{p}_o - \left(D_f^+\Delta p_{o,T_+} - D_f^-\Delta p_{o,T_-}\right)\right],\end{aligned} \tag{55}$$

$$\begin{aligned}\Delta\left(\frac{\mathbf{u}^h_{o,f}}{B_o}\cdot\mathbf{n}_f\right) = {} & \frac{-\mathscr{D}_{o,f}}{\mu_o B_o}\frac{dk_{ro}}{S_w}\Delta\widetilde{S}_w - \\ & +\frac{k_{ro}}{\mu_o B_o}\left[\left(\frac{\mathscr{D}_{o,f}}{\mu_o}\frac{d\mu_o}{dp_o} + \frac{\mathscr{D}_{o,f}}{B_o}\frac{dB_o}{dp_o}\right)\Delta\bar{p}_o - \left(D_f^+\Delta p_{o,T_+} - D_f^-\Delta p_{o,T_-}\right)\right],\end{aligned} \tag{56}$$

where

$$\mathscr{D}_{w,f} = D_f^+\left(p_o - p_c(S_w) - \rho_w g z\right)_{T_+} - D_f^-\left(p_o - p_c(S_w) - \rho_w g z\right)_{T_-},$$
$$\mathscr{D}_{o,f} = D_f^+\left(p_o - \rho_o g z\right)_{T_+} - D_f^-\left(p_o - \rho_o g z\right)_{T_-}.$$

We assume that coefficients $D_f^\pm$ are frozen at each Newton iteration. In this case the difference between the linear and nonlinear flux discretizations is only in the way we calculate $D_f^\pm$ for (55) and (56), but not in sparsity of Jacobian matrix.

For the fluxes in (43)-(45) and (52) we consider two flux discretization schemes. The upwinded saturation is obtained by using the nonlinear second-order upwind stabilization, presented in the first section.

Numerical experiments

The numerical experiments for steady-state diffusion and advection-diffusion problems in 3D can be found in (Danilov and Vassilevski 2009) and (Nikitin and Vassilevski 2010) respectively.

Here we present a few numerical results obtained with the new flux discretization and upwind approximation for the two-phase black oil model. The accuracy and the computational cost of the method are compared with the ones for the conventional linear two-point flux discretization.

In all test cases we considered pseudo-two-dimensional problems on $N\times N\times 1$ hexahedral meshes and used the following rock and fluid properties. Relative permeabilities of fluids $k_{r\alpha}$ are shown in Fig. 3 left. Capillary pressure p_c dependence on S_w is presented in Fig. 3 right. Viscosities μ_α and volume factors B_α are set by Table 1 and densities are $\rho_{w,0} \approx 4.331\cdot 10^{-1}$psi/ft and $\rho_{o,0} \approx 3.898\cdot 10^{-1}$psi/ft. The rock is assumed to be incompressible.

Both wells are incorporated through the bottom hole pressures. For injector it is $p_{\text{bh,inj}} = 4100$ psia and for producer $p_{\text{bh,pr}} = 3900$ psia. Well indexes are assumed to be fixed $WI = 10\,\frac{\text{bbl}\cdot\text{cp}}{\text{day}\cdot\text{psi}}$.

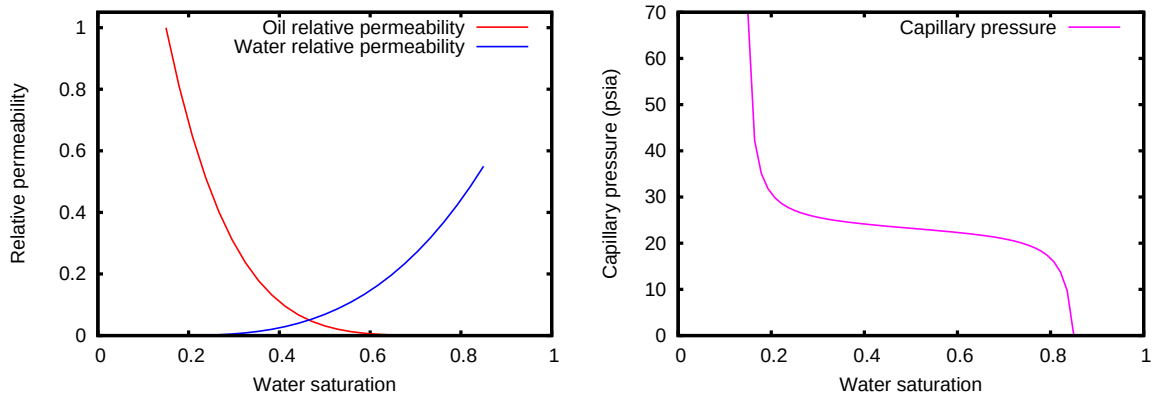

Figure 3 *Left: Oil and water relative permeabilities. Right: Capillary pressure dependence on S_w.*

p (psia)	B_o (bbl/STB)	B_w (bbl/STB)	μ_o (cp)	μ_w (cp)
3900	1.0030	1.01317	90.6	0.515
4000	1.0020	1.01291	96.0	0.518
4100	1.0009	1.01264	101.7	0.521

Table 1 *Fluid compressibility properties.*

Non-orthogonal grid

The main idea of the first experiment is the following. Take uniform $N \times N \times 1$ mesh. Fix the first and last two lines in order to leave well-connected cells intact. Rotate the central lines towards the wells (angle $\alpha = -30^\circ$) or away from them ($\alpha = 30^\circ$) and interpolate the other lines linearly between central lines and the boundary (see Fig. 4). Run simulation with linear and nonlinear flux discretization on modified mesh and compare the results with the ones on orthogonal mesh.

Permeability tensor is chosen to be $\mathbb{K} = \{100, 100, 10\}$.

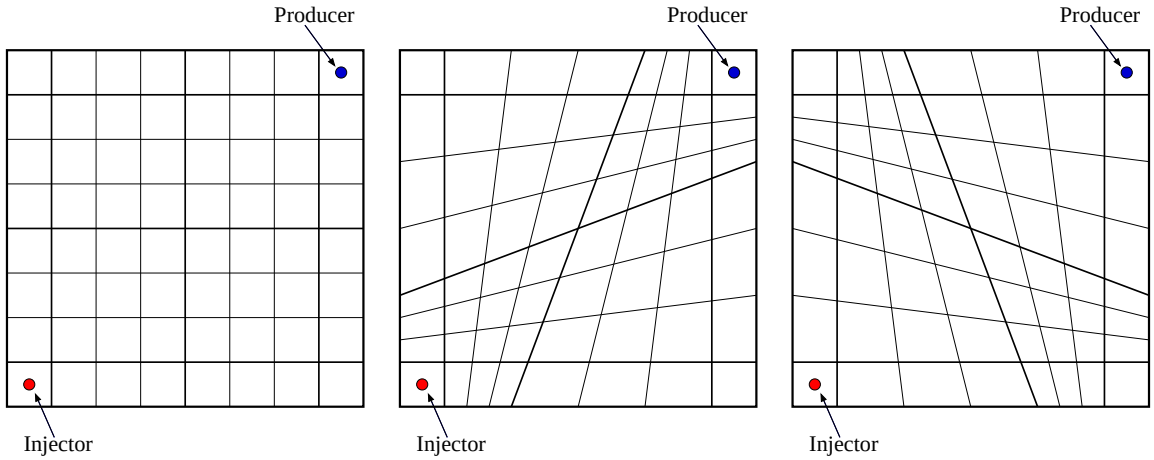

Figure 4 *Orthogonal and non-orthogonal sample grids.*

Figure 6 shows distribution of water saturation on the orthogonal grid (Fig. 6 left) and on grid M2 for linear (Fig. 6 center) and nonlinear (Fig. 6 right) flux disretizations. It can be easily seen that for linear discretization the form of the water front is different from the one on the orthogonal grid, while for nonlinear discretization the fronts are almost equal.

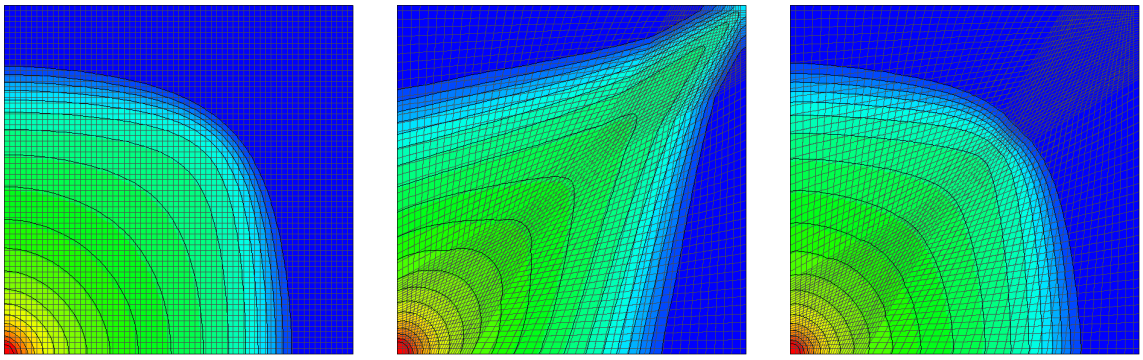

Grid M1
linear = nonlinear

Grid M2
linear

Grid M2
nonlinear

Figure 5 *Water saturation for grids M1 and M2 for the linear and nonlinear scheme at* $T = 250$ *days.*

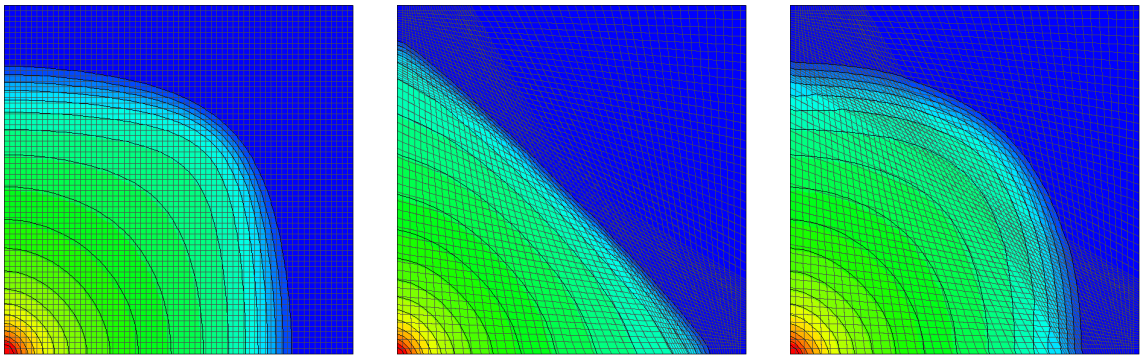

Grid M1
linear = nonlinear

Grid M3
linear

Grid M3
nonlinear

Figure 6 *Water saturation for grids M1 and M3 for the linear and nonlinear scheme at* $T = 250$ *days.*

Similarly the Figure 6 shows water saturations on the orthogonal grid (Fig. 6 left) and on grid M3 for linear (Fig. 6 center) and nonlinear (Fig. 6 right) flux disretizations. Again, nonlinear discretization provides the front which is very close to the front on the orthogonal grid, while linear one doesnâĂŹt preserve the behavior of the water front, that becomes flat.

The water breakthrough times are also noticeably different (see Table 2). Oil production rates are shown in Fig. 7, and water production rates are shown in Fig. 8. For grid M2 both linear and nonlinear fluxes break earlier than for grid M1, while for grid M3 both linear and nonlinear fluxes alternatively break later than for grid M1. Meanwhile the nonlinear discretization on the modified grids is very close to the one on the orthogonal grid.

	Grid 1	Grid 2	Grid 3
linear	372.2	224.1	564.2
nonlinear	372.2	362.2	388.5

Table 2 *Water breakthrough times. Non-orthogonal grid.*

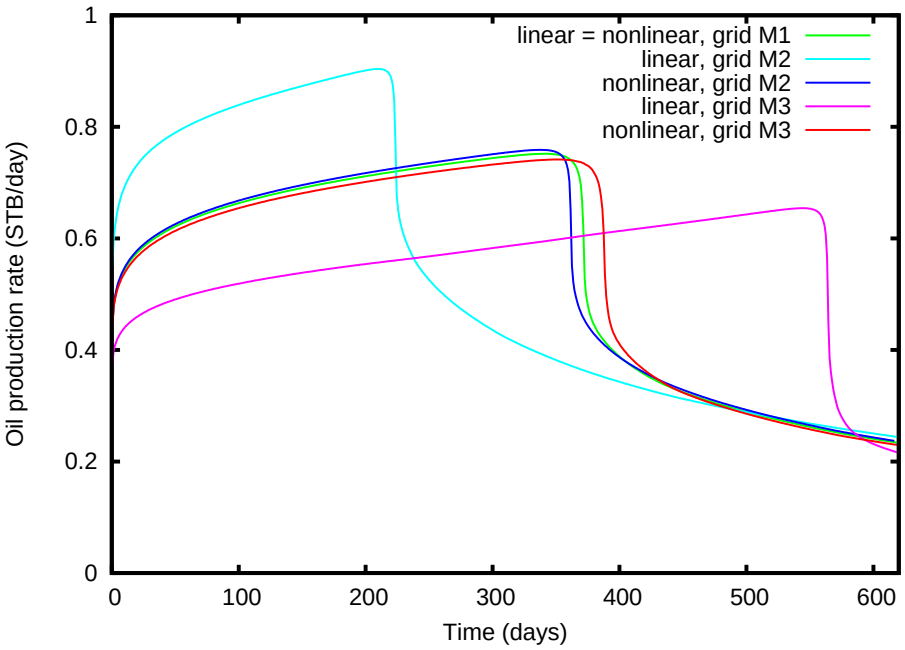

Figure 7 *Oil production rates for grids M1, M2 and M3.*

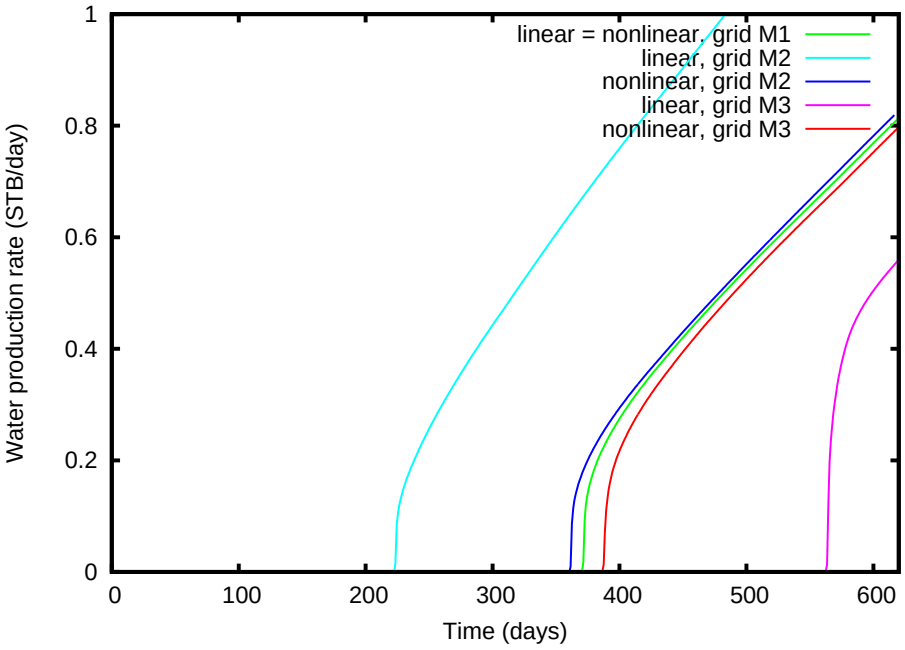

Figure 8 *Water production rates for grids M1, M2 and M3.*

Discontinuous tensor with high anisotropy

In the next experiment we use the uniform $64 \times 64 \times 1$ grid M1, but with a discontinuous full anisotropic permeability tensor (see Fig. 9).

$$\mathbb{K} = R_z(-\theta) \begin{pmatrix} 1000 & 0 & 0 \\ 0 & 10 & 0 \\ 0 & 0 & 10 \end{pmatrix} R_z(\theta), \qquad R_z(\theta) = \begin{pmatrix} \cos\theta & \sin\theta & 0 \\ -\sin\theta & \cos\theta & 0 \\ 0 & 0 & 1 \end{pmatrix}.$$

The computational domain is 100 ft $\times$ 100 ft, and rotation angle is the following:

$$\theta(S) = \begin{cases} 0^\circ & \text{if } 50 \text{ ft } \leq x+y < 100 \text{ ft}, \\ 90^\circ & \text{if } 100 \text{ ft } \leq x+y < 150 \text{ ft}, \\ 45^\circ & \text{if } x+y < 50 \text{ ft, or } x+y \geq 150 \text{ ft}. \end{cases}$$

Fig. 10 shows the water saturation field at the moment $T = 55$ days and Fig. 11 presents the oil pressure field at the moment $T = 10$. The front propagations are completely different even if discretizations differ only near wells, where $\theta = 45^\circ$. Oil and water production rates are shown in Fig. 12.

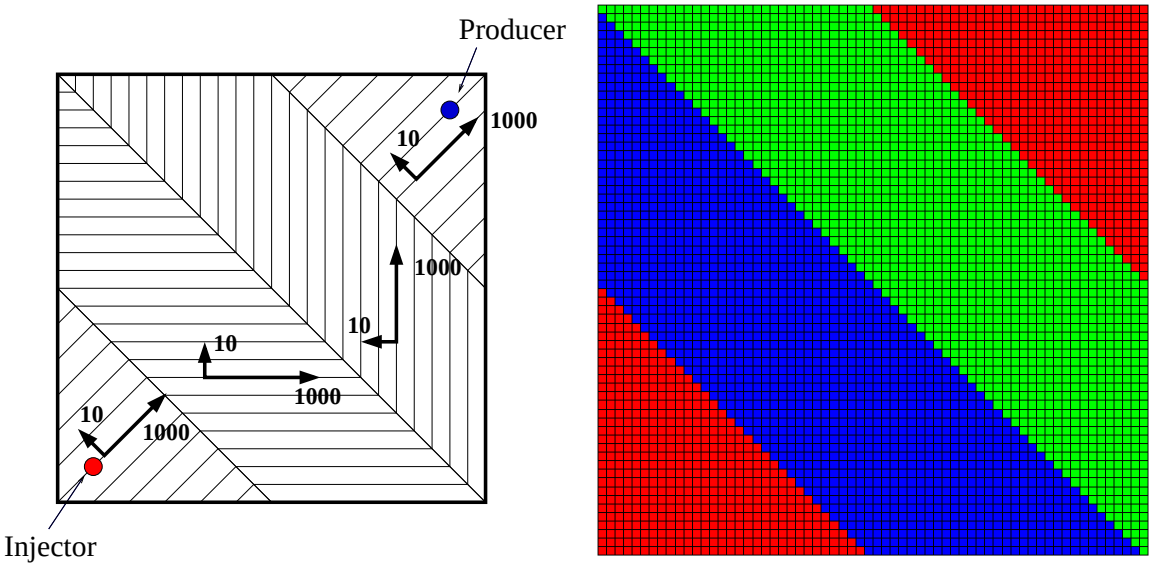

Figure 9 *Left: discontinuous anisotropic tensor. Right: sample mesh.*

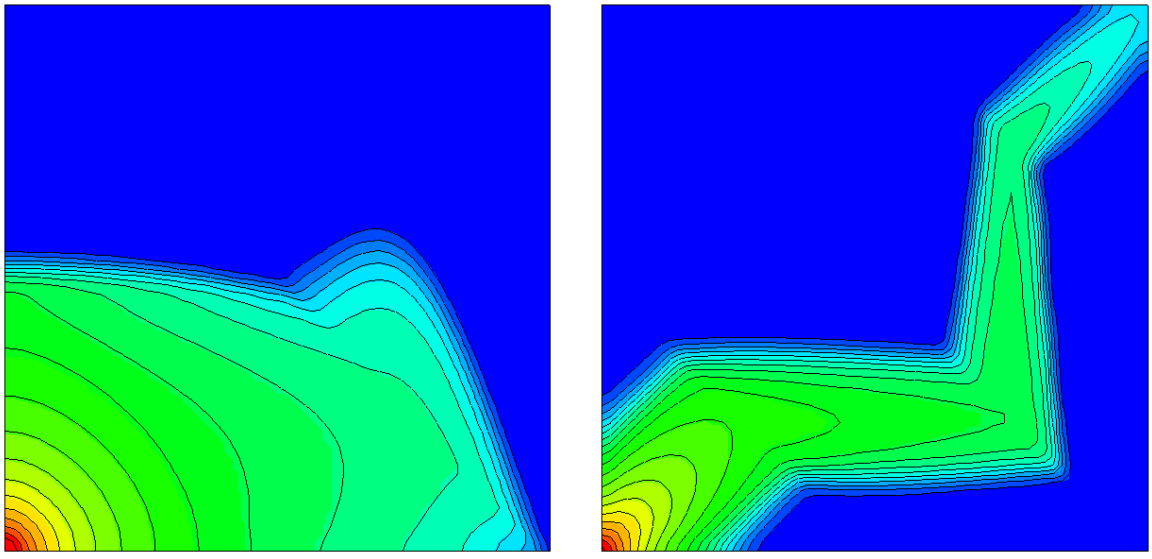

Figure 10 *Water saturation at $T = 55$ days. Discontinuous tensor with high anisotropy.*

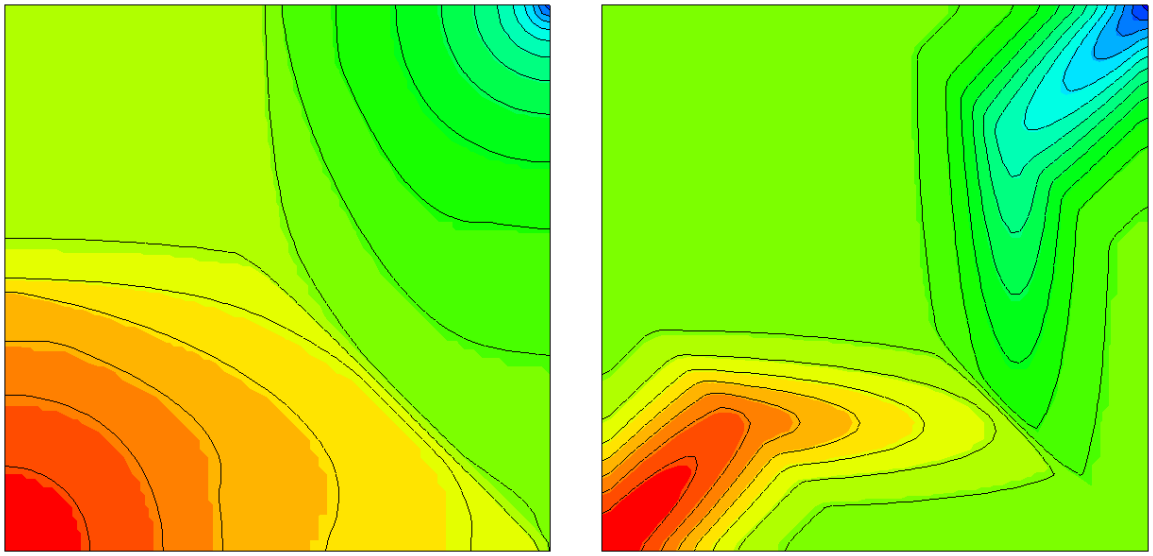

linear nonlinear

Figure 11 *Oil pressure at $T = 10$ days. Discontinuous tensor with high anisotropy.*

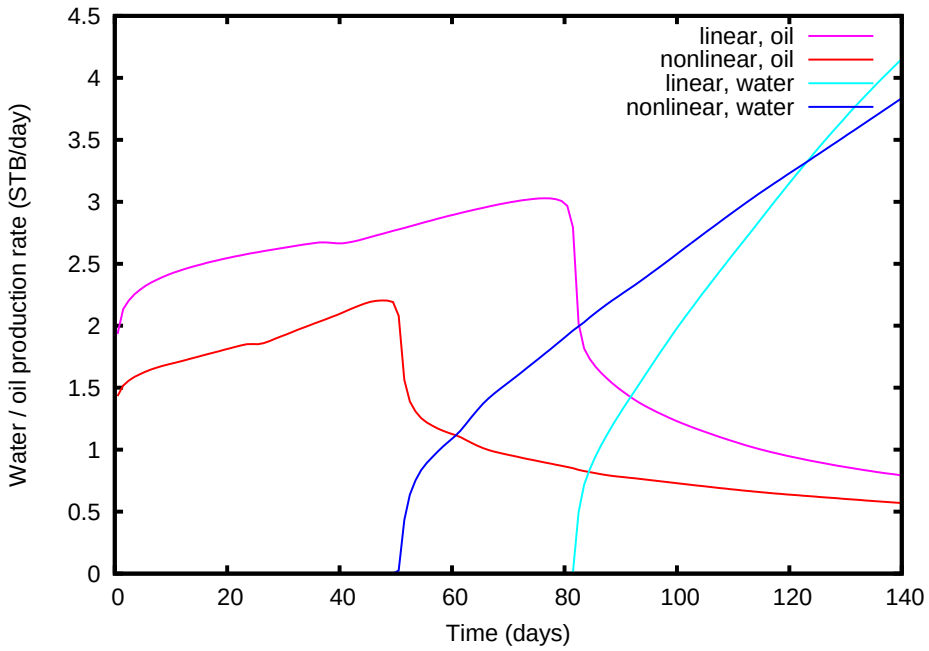

Figure 12 *Oil / water production rates. Discontinuous tensor with high anisotropy.*

Fully implicit scheme

We proceed to the numerical comparison of the impact of the nonlinear and linear flux discretizations to the convergence of the Newton method for the fully implicit scheme presented in the second section. We confine ourselves by nonlinearities coming from the relative permeabilities, viscosities and flux coefficients (for nonlinear discretizations). In the comparison we neglect nonlinearity generated by the rock and fluids compressibilities and the capillary pressure.

We consider the simulation of water injection and oil production on grid M3 from the first experiment. Table 3 presents CPU times and numbers of Newton iterations for 200 day simulation with different time steps (from 1 to 20 days) and stopping criterion $\varepsilon_{\text{nwt}} = 10^{-3}$. We observe that both the compu-

	Linear			Nonlinear		
Δt (N)	time	#it	#it/N	time	#it	#it/N
1.0 (200)	111s	369	1.8	120s	422	2.1
2.0 (100)	69s	211	2.1	99s	328	3.3
4.0 (50)	51s	140	2.8	76s	233	5.7
8.0 (25)	35s	86	3.4	59s	168	6.7
20.0 (10)	25s	49	4.9	46s	122	12.2

Table 3 *Time step, (N – number of steps), CPU time (sec) and the total number of Newton iterations (#it.),* $\varepsilon_{\text{nwt}} = 10^{-3}$.

tational work (time) and the total number of Newton iterations (#it) are higher for the nonlinear flux discretization than those produced by the conventional linear fluxes. The increase of the time step reduces the computation time, but the average number of iterations per time step grows. For the smaller time steps the total CPU time and total number of iterations are only 20% higher for the nonlinear flux discretization than for the linear one. For the bigger steps, however, the difference is larger - 2.5 times.

	Linear			Nonlinear		
Δt (N)	time	#it	#it/N	time	#it	#it/N
1.0 (200)	122s	412	2.1	206s	738	3.7
2.0 (100)	79s	247	2.5	159s	558	5.6
4.0 (50)	54s	158	3.1	123s	420	8.4
8.0 (25)	38s	94	3.8	97s	304	12.2
20.0 (10)	26s	53	5.3	65s	182	18.2

Table 4 *Time step, (N – number of steps), CPU time (sec) and the total number of Newton iterations (#it.),* $\varepsilon_{\text{nwt}} = 10^{-4}$.

Table 4 presents CPU times and numbers of Newton iterations for 200 day simulation with different time steps (from 1 to 20 days) and stopping criterion $\varepsilon_{\text{nwt}} = 10^{-4}$. One can see the use of the nonlinear discretization makes the residual of the Newtom method to drop slower, and the difference between linear and nonlinear discretizations becomes more noticeable: extra 75% for small time steps and up to 3.5 times for the big ones.

The time measurements presented in tables 3, 4 indicate that the computational cost of each Newton iteration is the same for both linear and nonlinear discretizations.

Conclusions

We presented here the new monotone cell-centered finite volume method. Its monotonicity is understood as non-negative approximations of non-negative solutions to partial differential equations, but it can be easily modified to provide the discrete maximum principle.

The cornerstones of the method are the nonlinear two-point flux discretization and the second order upwind approximation. Numerical experiments with the two-phase black oil model demonstrate its superiority to the conventional linear two-point flux discretization.

For orthogonal grids with isotropic or grid-aligned anisotropic permeability tensor, the nonlinear two-point flux discretization is identical to the conventional linear two-point flux discretization. However, in case of non-orthogonal grid or full anisotropic permeability tensor, the nonlinear two-point flux discretization provides more accurate and physically relevant front propagation and water breakthrough time than the conventional linear two-point flux discretization. The computational work for the new method is noticeably higher for IMPES due to the use of Picard iterations, yet just slightly higher for fully implicit method due to the larger number of Newton iterations.

Acknowledgements

This work has been supported in part by RFBR grants 11-01-00971, 12-01-31275, ExxonMobil Upstream Research Company, Federal program "Scientific and scientific-pedagogical personnel of innovative Russia" and project "Breakthrough".

References

[Aavatsmark et al. 2008] Aavatsmark, I., Eigestad, G., Mallison, B., Nordbotten, J. [2008] A compact multipoint flux approximation method with improved robustness, *Numerical Methods for Partial Differential Equations* **24** (5), 1329–1360.

[Aziz and Settari 1979] Aziz, K. and Settari, A. [1979] *Petroleum Reservoir Simulation.* London: Applied Sci. Publ. Ltd.

[Brezzi and Fortin 1991] Brezzi, F. and Fortin, M. [1991] *Mixed and Hybrid Finite Element Methods*, New York: Springer-Verlag

[Chen et al. 2006] Chen, Z., Huan, G. and Ma, Y. [2006] *Computational Methods for Multiphase Flows in Porous Media.*, SIAM.

[Danilov and Vassilevski 2009] Danilov, A. and Vassilevski Yu. [2009] A monotone nonlinear finite volume method for diffusion equations on conformal polyhedral meshes. *Russian J. Numer. Anal. Math. Modelling*, **24** (3), 207–227.

[Kapyrin 2007] Kapyrin, I. [2007] A family of monotone methods for the numerical solution of three-dimensional diffusion problems on unstructured tetrahedral meshes, *Doklady Mathematics* **76** (2), 734–738.

[LePotier 2005] LePotier, C. [2005] Schema volumes finis monotone pour des operateurs de diffusion fortement anisotropes sur des maillages de triangle non structures, *C.C.Acad. Sci. Paris* **341**, 787–792.

[Lipnikov and Gyrya 2008] Lipnikov, K. and Gyrya, V. [2008] High-order mimetic finite difference method for diffusion problem on polygonal meshes, *J. Comp. Phys.* **227**, 8841–8854

[Lipnikov et al. 2007] Lipnikov, K., Svyatskiy, D., Shashkov, M. and Vassilevski, Y. [2007] Monotone finite volume schemes for diffusion equations on unstructured triangular and shape-regular polygonal meshes, *J. Comp. Phys.* **227**, 492–512.

[Lipnikov et al. 2009] Lipnikov, K., Svyatskiy, D. and Vassilevski, Y. [2009] Interpolation-free monotone finite volume method for diffusion equations on polygonal meshes, *J. Comp. Phys.* **228** (3), 703–716.

[Lipnikov et al. 2010] Lipnikov, K., Svyatskiy, D. and Vassilevski, Y. [2010] A monotone finite volume method for advection-diffusion equations on unstructured polygonal meshes, *J. Comp. Phys.* **229**, 4017–4032.

[Lipnikov et al. 2012] Lipnikov, K., Svyatskiy, D. and Vassilevski, Y. [2012] Minimal stencil finite volume scheme with the discrete maximum principle, *Russian J. Numer. Anal. Math. Modelling*, **27** (4), 369–385.

[Nikitin and Vassilevski 2010] Nikitin, K. and Vassilevski, Yu. [2010] A monotone nonlinear finite volume method for advection-diffusion equations on unstructured polyhedral meshes in 3D, *Russian J. Numer. Anal. Math. Modelling*, **25** (4), 335–358.

[Nikitin 2010] Nikitin, K. [2010] Nonlinear finite volume method for two-phase flow in porous media (in Russian), *Mathematical Modelling*, **22** (11), 131–147.

[Peaceman 1978] Peaceman, D. W. [1978] Interpretation of Well-Block Pressures in Numerical Reservoir Simulation. *SPEJ* June, 183–194.

[Vassilevski and Kapyrin 2008] Vassilevski, Yu. and Kapyrin, I. [2008] Two splitting schemes for nonstationary convection-diffusion problems on tetrahedral meshes, *Comp. Math. and Math. Phys.* **48** (8), 1349–1366.

[Yuan and Sheng 2008] Yuan, A. and Sheng, Z. [2008] Monotone finite volume schemes for diffusion equations on polygonal meshes, *J. Comp. Phys.* **227** (12), 6288–6312.